Robust distance protection for cross-country faults in power grids with high penetration of inverter- based resources

Chavez, Jose de Jesus; Popov, Marjan; López, David; Terzija, Vladimir; Azizi, Sadegh

DOI
10.1016/j.prime.2024.100708

Publication date
2024

Document Version
Final published version

Published in
e-Prime - Advances in Electrical Engineering, Electronics and Energy

e-Prime - Advances in Electrical Engineering, Electronics and Energy 9 (2024) 100708

Contents lists available at ScienceDirect

e-Prime - Advances in Electrical Engineering, Electronics and Energy

journal homepage: www.elsevier.com/locate/prime

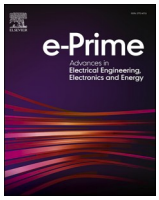

Robust distance protection for cross-country faults in power grids with high penetration of inverter- based resources

Jose de Jesus Chavez [a,b,*], Marjan Popov [b], David López [c], Vladimir Terzija [d], Sadegh Azizi [e]

[a] Tecnológico de Monterrey, Escuela de Ingeniería y Ciencias, Av. General Ramón Corona 2514, Zapopan, Jalisco 45138, Mexico
[b] Faculty of EEMCS, Delft University of Technology Delft, 2628 CD Delft, the Netherlands
[c] Redinter Chile, Isidora Goyenechea 3000, oficina 1602, Las Condes, Santiago, Chile
[d] Newcastle University School of Engineering, Merz Court, E4.41, Newcastle upon Tyne NE1 7RU, United Kingdom
[e] School of Electronic and Electrical Engineering, University of Leeds, LS2 9JT, Leeds, United Kingdom

ARTICLE INFO

Keywords:
Distance protection
Fault detector
Faulty phase selector
Stockwell transform
Real-time digital simulations

ABSTRACT

Cross-country faults can adversely affect the operation of protection devices. Relays whose pickup is based on overcurrent or impedance elements are more likely to fail during cross-country faults. The failure can be expressed as an unnecessary trip of all phases during a single-phase fault or even blocked relay functions. Relays may also fail to operate due to low fault currents, which is the case when power grids make use of many inverter-based resources (IBR) or when two simultaneous faults occur in the same phase and in different locations. This paper proposes a Recursive Discrete Stockwell Transform (RDST) method for addressing the mentioned challenges. The energy content computed by the RDST is used for fault detection and faulty phase selection. A robust distance relay model is proposed to ensure correct relay performance and is combined with a directional and an impedance trajectory module. The proposed method performance is thoroughly evaluated by applying real-time simulations for 6480 different cross-country faults, including three repetitions, four different generators (Synchronous generators, Wind turbine type-III, Wind turbine type-IV), two rating powers, three different fault distances, five different types of faults, and six grid codes. Ninety cases are also tested with real devices in hardware in the loop. Simulation results confirm the method's ability to detect different fault types, even during low fault currents, and to ensure high accuracy in phase selection.

1. Introduction

To transport electricity, transmission power grids usually use single-circuit three-phase lines. Two or more parallel lines are also extensively used to increase power transport capacity. Parallel lines on the same tower may take part of circuits with different voltage levels, and such arrangements produce strong magnetic coupling. The mutual impedances that result from these coupling may have values which are even 70 % of the self-impedance. The mutual impedance of the lines can jeopardize the operation of protection devices, especially during cross-country faults (CCFs). CCFs are defined as earthed faults occurring in different phases of the same circuit at different locations, simultaneously or at different moments. A failure in the operation of distance relays during CCFs may lead to three-phase trips in both circuits of the parallel line configuration. The effect of this failure can be very severe under stressed conditions.

Creating protection algorithms for CCFs is challenging, and so far, some attempts have been made to overcome the above challenges. Distance modules may produce selective tripping by themselves. Usually, this module uses voltage self-polarization to obtain a reliable voltage to compare the impedance of the fault. During single-circuit conditions, they can distinguish the faulty phase; however, during CCF, detecting the faulty phase is not easy, and the module may fail to determine the fault correctly. This may happen because of the change in impedance, and healthy elements are prone to maloperation. Also, they are unreliable for zero-voltage faults. In that sense, fault selector supervision is necessary. Above others, some methods used for fault selector are overcurrent, voltage, frequency wave information, delta quantities, and sequence information [1–4]. Certainly, those methods can determine the faulty face but also have drawbacks such as lack of self-adaptation, loss of sensitivity in the presence of fault current limiters or high impedance, low sensitivity due to non-significant voltage drop,

* Corresponding author at: Tecnológico de Monterrey, Escuela de Ingeniería y Ciencias, Av. General Ramón Corona 2514, Zapopan, Jalisco 45138, Mexico.
E-mail address: j.j.chavezmuro@tec.mx (J.J. Chavez).

https://doi.org/10.1016/j.prime.2024.100708
Received 16 November 2023; Received in revised form 1 July 2024; Accepted 11 July 2024
Available online 27 July 2024

reliability issues may appear once speed detection is the priority. The impact of CCFs in a double-circuit line on the performance of the current differential relay has been evaluated in Solak and Rebizant [5], it has been pointed out that relays may trip external faults incorrectly or may not trip internal faults. At the same time, the CCFs effects on distance relay in a 132 kV double circuit with two different voltages power grid were analyzed in Zin et al. [6], the CCFs effects on distance relay in a 132 kV double circuit with two different voltages power grid were analyzed. In [7,8], a comprehensive description of grounded and ungrounded CCFs in a parallel transmission line is reported; the mutual coupling in a double circuit is highlighted as an adverse effect relays that may overreach faults, a solution using zero-sequence voltage and current is proposed. This method is effective for networks with only synchronous generators, and the effect of IBRs is not considered. Recently, more sophisticated techniques, such as the Maxima Overlap Discrete Transform, have been used to detect and classify CCFs [9] even during power swings. In [10], relay polarization has been recognized as a drawback during CCFs. A summary of the improvements in protective functions and commercial relays to cover CCFs is reported in Venkatesh and Voloh [11]. However, these techniques are suitable for detecting the faulty phase; they work on systems with only Synchronous generators. In addition, they need a high computational burden; CCFs can also occur in medium-voltage power grids, making this subject equally challenging [12]. Including flexible AC transmission systems based compensating has introduced harmonics and non-linearity in power systems, causing fast changes in the line impedance. As a result, the current and impedance-based distance relaying scheme has limitations. These methods are summarised in Biswas and Nayak [13], where the pros and cons are highlighted and compared, and a case study is proposed. However, there is no information about IBRs. In [14,15], the protection issues when IBRs are connected are well established and summarized. In [16], it is revealed that classical methods misidentify the fault type in microgrids that include photovoltaic distributed generations. To overcome that problem, two classifiers have proposed methods with a low computational burden. Knowing the problem in phase selector modules when IBRs are near, some authors [18] proposed to manipulate the control of the IBRs to make the sequence current angles similar to those obtained when the system is fed by synchronous generators only. Recently, artificial intelligence has been used to overcome the drawbacks of the methodologies when IBRs are near the relays, such as in Biswas et al. [20], where a dual time transform is used to extract the data from the electrical signals, currents and voltages, and classify by a decision tree. The same authors went forward and used convolution neural networks to improve the performance of relays under conditions of IBRs and FACTs compensated lines [21]. Other authors use more traditional techniques to overcome issues when IBRs are in the net, such as [22], where a fault classifier based on symmetrical components of the local voltage and current during asymmetrical faults is used with excellent results. The methods perform well but have not been tested in cross-country fault cases.

This paper proposes a robust distance protection method to address some challenges related to CCFs in power grids with high penetration of inverter-based resources (IBR), such as phase selector and fault detection. The relay model is designed in such a way to deal not only with classical faults but also with CCFs. The relay comprises four modules: fault detection, faulty phase selection, directionality, and distance detection. Fault detection (pickup) is the first module. It is based on the Stockwell Energy (SE) obtained by computing the Stockwell transform (ST) from the current signals. The authors in Chavez et al. [23] already presented this technique. This paper proposes a Recursive Discrete Stockwell Transform (RDST) method to compute SE. The resulting SE is defined in both time and frequency domains. In the frequency domain, a two-dimensional Gaussian filter is used to magnify non-fundamental frequency signals. As a result, the fault detector performs well even when the fault current is limited. The second module, the faulty phase selector, is also based on the SE. The magnitudes of the SE per fault loop (A, B, C, AB, BC, and CA) are applied to determine precisely the fault type. The module also efficiently determines ground faults. The third module is the directionality module used to determine the fault in the forward or reverse direction. The fourth module is the distance determination module. Several CCF cases for a parallel line with identical characteristics are analyzed. The nearby transformers are solidly grounded. CCFs in ungrounded and other system configurations are out of the scope of this paper. All cases are simulated by applying an automatic script programmed in the real-time simulator to execute automatically numerous test cases. The results prove the effectiveness of the relay performance during cross-country faults.

2. Methodology

This section summarizes the procedure for obtaining SE and introduces the Recursive Discrete Stockwell Transform (RDST) to alleviate the computational burden.

2.1. Fast discrete Stockwell transform (FDST)

The FDST of a discrete-time signal $x[nT]$, $n = 1,\ldots,N$ can be expressed as:

$$S_{(jT,\eta NT)} = \sum_{m=1}^{N} [\mathbf{H}\circ\mathbf{Gw}]\cdot e^{j2\pi mn/N} \tag{1}$$

where m and n represent the frequency and time point indices of the window ($n = 1,2,\ldots,N$) respectively. Matrix $\boldsymbol{H}$ in (2) is built by using the Discrete Fourier coefficients from the signal $x[kT]$ arranged in a concatenate and rotated matrix as:

$$\mathbf{H}_{M\times N} = \begin{bmatrix} X_2 & X_3 & \cdots & X_N & X_1 \\ X_3 & X_4 & \cdots & X_1 & X_2 \\ \vdots & \vdots & & \vdots & \vdots \\ X_{M+1} & X_{M+2} & \cdots & X_{M-1} & X_M \end{bmatrix} \tag{2}$$

where M is equal to $N/2$, matrix $\boldsymbol{Gw}$ in (1) is a two-dimensional Gaussian window [24], tuned for localization in frequency and time domains.

Matrix $\boldsymbol{H}$ is multiplied by $\boldsymbol{Gw}$ using the Hadamard product. The resulting summation of the dot product ($[\mathbf{H}\circ\mathbf{Gw}]\cdot e^{i2\pi mn/N}$) in (1) corresponds to the Inverse Discrete Fourier transform (IDFT). In that sense, all the DFT properties can be exploited to reduce the number of equations. When the data window has a size power of two, the IDFT can be accelerated considerably by an IFFT algorithm, decreasing the computational burden. The resulting ST matrix consists of the instantaneous phasor values for each frequency in the range of 1 to M.

2.2. Recursive discrete Stockwell transform

Deriving the ST matrix for each window using the FFT may increase the processing cost. Thus, a recursive procedure is proposed to get the Stockwell Transform, decreasing the computational burden and increasing the computation speed. In (2), the parameter Xn denotes the nth frequency component obtained using the DFT; thus for a history window k, as shown in Fig. 1, the DFT expression is:

$$X_n[k] = \sum_{l=k-N+1}^{k} x[l] W_N^{n(N+l-k-1)} \tag{3}$$

while for an actual window $k-1$ is

$$X_n[k-1] = \sum_{l=k-N}^{k-1} x[l] W_N^{n(N+l-k)} \tag{4}$$

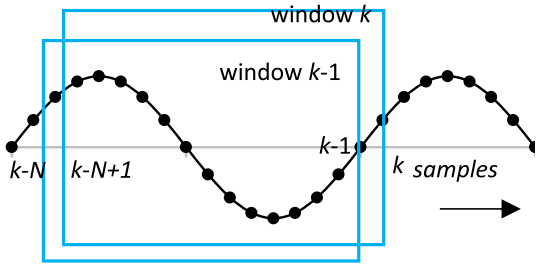

Fig. 1. Two consecutive data windows to depict the recursive process in time.

$$W_N^{-n}X_n[k-1] = \sum_{l=k-N+1}^{k} x[l]W_N^{n(N+l-k-1)} + W_N^{-n}(x[k-N]-x[k]) \quad (5)$$

According to Fig. 1, the window under analysis in (4) is $l = k-m$, $n = 0, \ldots, N-1$, and $W_N = e^{-j2\pi/N}$. Multiplying (4) by W_N^{-n}, the equation can be rearranged as

Expression (5) is the DFT of the kth window, as shown in (3). By rearranging (5) by applying (3), the X_n components of matrix $\boldsymbol{H}$ can be obtained more easily:

$$X_n[k] = W_N^{-k}(X_n[k-1] + x[k] - x[k-N]) \quad (6)$$

A similar procedure is done to obtain ST coefficients ($S_n[k]$). After the ST for the first window is computed by (1), the rest of the nth frequencies and the kth+1windows are computed by:

$$S_n[k] = W_N^k\left(\begin{matrix}S_n[k-1]+\\(\mathbf{H}_n\mathbf{Gw}_n[k]-\mathbf{H}_n\mathbf{Gw}_n[k-N])/N\end{matrix}\right) \quad (7)$$

The consecutive data window is moving in time but not in frequency, as seen in Fig. 2. Therefore, by using (6) and (7), the computational burden decreases for each window after the kth+1 which helps to avoid unnecessary computations (see Table 1 for the atomic math operations). The recursive DFT has been widely used in research and commercial relays. Nevertheless, one of the innovations presented in this paper corresponds to the use of the recursive ST, where the recursive DFT is part of the process.

2.3. 2D Gaussian windows

The Gaussian window translates any transient frequency and scales it individually. The Gaussian window is defined as:

$$\mathbf{Gw}_{(m,n)} = e^{T1} + e^{T2} \quad (8)$$

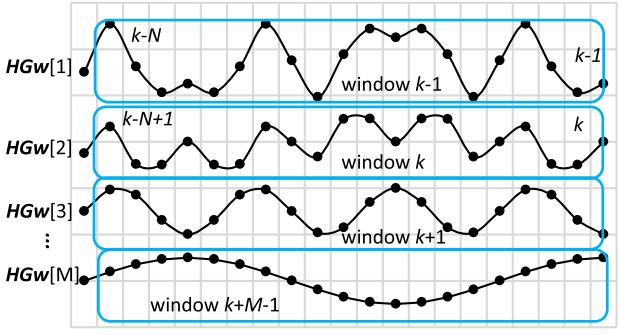

Fig. 2. Illustrated points used in the Hadamard product of ***HG***.

Table 1
. Atomic math operations performer in the Stockwell transform and its versions.

Method	Number of additions	Number of multiplications
Discrete Stockwell transform [24]	$\frac{N}{2}\left((N-1)\times(N+2)\right)$	$\frac{N^2}{2}(N+4)$
Fast Discrete Stockwell transform (Radix-R) [25]	$\frac{N}{2}\left(N(N+2)\times\log_R(N)\right)$	$\frac{N}{2}\left(2N+\log_R(N)(1+N)\right)$
Recursive discrete Stockwell	1st equal to Fast Discrete Stockwell transform from 2nd $(2/3)N+2$	1st equal to Fast Discrete Stockwell transform From 2nd $(6N+N^2)/4$

where

$$T_1 = k_G(n-1)^2, \quad T_2 = k_G(N-n+1)^2, \quad k_G = -\frac{2\pi^2 F}{(a+bm^c)^2}, \quad (9)$$

It is not obvious how to pick the values of the Gaussian filter; however, F is a factor that mainly controls the central window values, making the shape of the window concave or convex. Parameter a also varies the shape of the window but to a lesser extent. Parameter b ranges from 1 to 0, providing a bandpass swelling (or decreases when it is small) in the center of the window. It also damps the oscillations by smoothing the edges of the windows. Parameter c varies between 0 and 1, contributing to capturing damped hidden frequencies. To determine the Stockwell Energy (SE), the set of the window length and the number of samples should be set appropriately. Empirical analysis has shown that setting the window parameters $F = 0.01$, $a = 4.5$, $b = 0.9$, and $c = 0.2$ is the most suitable for events such as faults in the presence of sources used with IBRs. Fig. 3 shows the window and highlights the impact of the adjustment of each factor. The 2D Gaussian window operates satisfactorily in magnifying ST coefficients for the vast majority of electromagnetic transients. Nevertheless, the user can tune the filter differently to improve the ST performance during certain transients.

2.4. Stockwell energy

The ST generates a two-dimensional signal array, defined concurrently in the time and the frequency domain. From the generated array, the SE is computed by using the Parseval Theorem for a 2D discrete signal. Then, the energy of the ST matrix calculated by (7) is:

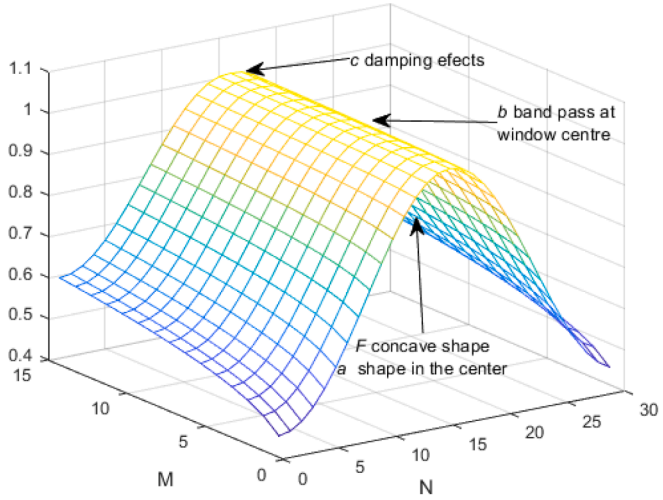

Fig. 3. Illustrative 30-points Gaussian windows. F, a, b and c are the parameters that control the filter as explained in Section 2.3 (values of $F = 0.01$, $a = 4.5$, $b = 0.9$ and $c = 0.2$).

$$SE(t) = \sum_{m=0}^{M-1} \sum_{n=0}^{N-1} \left| S_{(m,n)} \right|^2 \tag{10}$$

Because the ST is defined in time and frequency domains, the SE's changes its magnitude with the time or frequency change. The SE increase is more significant than the changes in one-dimensional energy signals [25] and therefore, during disturbances, the indicator is more sensitive. The SE is computed by adding the absolute square value of the ST matrix. Thus, the 2D energy of the current is expressed in amperes to the power of four (A^4). The data window adjustability, the ideal time, and the frequency resolution make the SE an excellent indicator for low-value fault currents [23].

3. Distance relay modeling

This section describes the distance relay model, which is enhanced by applying SE for the fault detector and the faulty phase selector modules. The other two modules, directionality and distance computation modules, are modeled according to [26,27]. The flow chart of the enhanced relay is shown in Fig. 4, where a dashed blue line highlights the proposed modules. The relay only generates a trip command when the fault is in Zone-1 or Zone-2. The use of ST overcomes two persistent problems occurring in overcurrent and impedance relays during CCFs. The first one is that the control of IBRs limits the short-circuit current, and therefore, distance relay experiences difficulties with picking up a fault [23]. Secondly, a method based on the SE is used to supervise the faulty phase selection. During CCFs, the relay operation may result in incorrect phase selection or direction determination, leading to a three-phase switching [6,7]. To ensure fault identification all the modules must operate at the same time range for at least three consecutive samples.

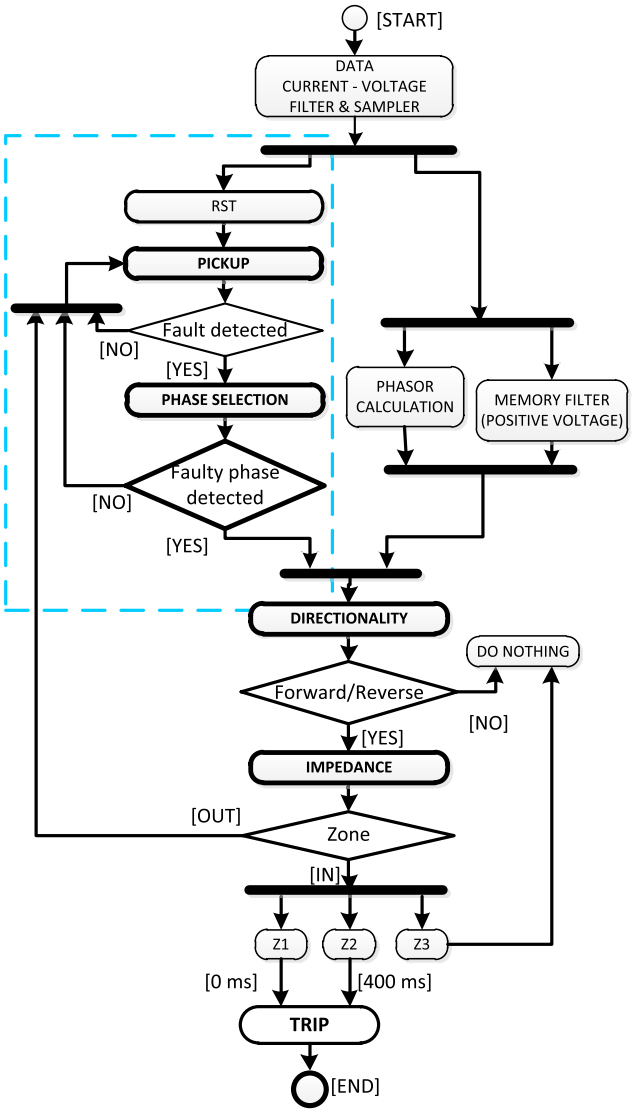

Fig. 4. Proposed distance protection relay flowchart with the SE indicators highlighted Faulty phase selection logic.

3.1. Fault detection supervision by the Stockwell energy

The distance module itself can identify numerous faults. However, many others must be correctly identified. Thus, the distance relays do not operate based on the impedance trajectory module alone. The first module of the distance relay is the fault detector. The module detects a faulty condition in the power grid and starts the corresponding functions for selective fault clearance, such as:

- determination of the faulted phases (loops),
- enabling direction determination,
- enabling impedance calculation,
- enabling of trip command,
- other functions.

The SE is monitored per phase and used to start up the relay. A signal output one is generated when the threshold value is exceeded. The threshold value is set using the steady-state SE value plus 5 % to include the harmonic distortion allowed and 10 % to add a safety margin. Hence, the limit is:

$$SE_{Limit} = SE + 0.05SE + 0.1SE \tag{11}$$

The SE steady-state parameter adjusts its value based on the system's prevailing conditions every 2 s, making the SE module adaptive. Computing the SE energy according to actual conditions helps avoid relay miss operations during events that are not considered faults.

3.2. Faulty phase selection supervision by the Stockwell energy

The proposed method of faulty phase selection is a high-speed process that starts after the fault is detected. The faulty type (single fault $FT = 1$, double fault $FT = 2$, or three-phase fault $FT = 3$) is determined by (12).

$$FT[k] = \text{round}\left(\frac{SE_A[k] + SE_B[k] + SE_C[k]}{\max(SE_A[k], SE_B[k], SE_C[k])}\right) \tag{12}$$

It is crucial to know if the fault also involves the ground, and therefore, the angle of Xk in (2) is observed. For ground faults, the values of the angles ($XA_{k,1}$, $XB_{k,1}$, and $XC_{k,1}$) are fixed; 0 or π value. For non-grounded faults, the angles vary from 0 to π. In this way, by using the angle information and

$$\left.\begin{array}{l} if \left\{ \begin{array}{l} \measuredangle\left(X_{A,B,C}(k-M)\right) = \\ \measuredangle\left(X_{A,B,C}(k-(M-1))\right) = \ldots \measuredangle\left(X_{A,B,C}(k)\right) \end{array} \right\} \\ GrX[k] = 1; \quad else \quad GrX[k] = 0 \end{array}\right. \tag{13}$$

the "IF" statement in (13), grounded faults are identified.

The angle variation enables the fault selector to detect different fault types at slightly different times. To overcome this possible problem, the phase selection is delayed sufficiently to allow the evolvement of the fault. The fault type selection priority is a three-phase fault after three consecutive detections. Other fault types are released immediately after, with a slight delay of five samples, to ensure the detection of ungrounded or grounded faults. The decision logic is shown in Fig. 5.

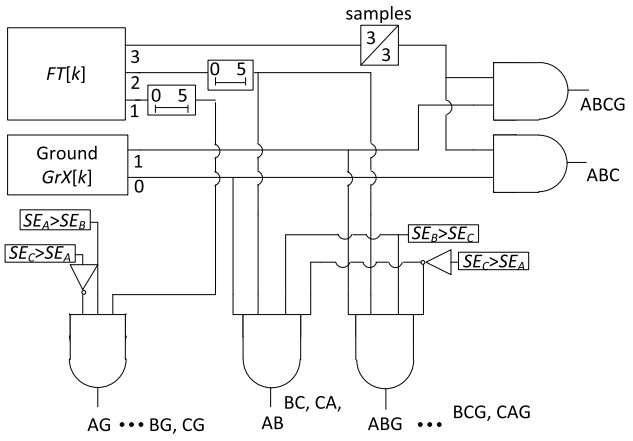

Fig. 5. Faulty phase selection logic.

3.3. Directionality and impedance determination

In order to design a full relay model, as seen in Fig. 4, directionality and impedance modules are needed. For the directionality, the fault current and the positive polarization voltage (VAB+*, VBC+*, VCA+*) are used to compute the directional indicators (zero, negative, and zero vs negative). For the impedance trajectory, the quadrilateral characteristic is applied (as reported in [26,27]).

4. Study case in real-time

This paper uses the modified benchmark model proposed in the Horizon 2020 MIGRATE project [28]. The system comprises detailed EMT models for Type-3 and Type-4 WTs, PV plants, and HVDC links. See Appendix A for major details about IBRs and Appendix B for the transmission line configuration. The impact of IBR is such that faults remain undetected in some cases [23]. The system is entirely modeled in a real-time digital simulation (RTDS) environment by using small time steps for the converters and standard time steps for the rest of the elements; 2.5 μs, and 50 μs, respectively.

4.1. Study case details

CCFs are more likely to occur on parallel lines located at the same tower. Therefore, the illustrated system in Fig. 6 has been used for this occasion. Because a double-phase fault produces a three-phase trip, only LN faults in LINE-I (L-I) are analyzed. The variables are:

- Infeed power of 40 MW or 200 MW delivered by the Wind Turbine (WT) type-3, type-IV (which means 32.5 % or 70 % of IBRs power penetration) or Synchronous Generator (SG) connected to Bus 6.
- Fault distance of 10 %, 75 %, and 90 % in L-I, and Fixed fault distance of 50 % in LINE-II (L-II) concerning Bus 6.

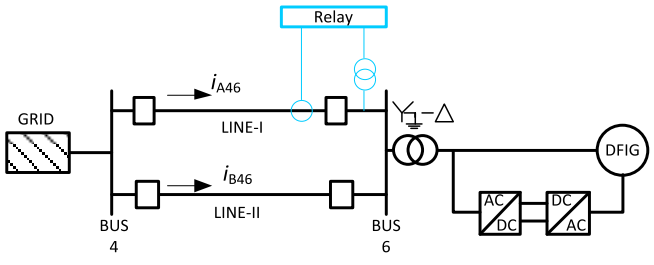

Fig. 6. The MIGRATE reduced and modified system used as a study case.

- Fault types: AG-BG, AG-CG, AG-AB, AG-BC, and AG-ABCG, at L-I and L-II, respectively.
- Fault times are same time instants in both lines, fault at L-II 0.1 s before a fault at L-I, and fault at L-II 0.1 s after a fault at L-I. This paper refers to the cases as 0 s, 0.1 s, and −0.1 s, respectively.
- Three repetitions for each case.

The fault impedance and the angle inception are set to 0.001 Ω and 0°, respectively. The trips in Zone-2 are delayed by 0.4 s, and Zone-3 is disabled. Every test is repeated three times to ensure the behavior of the relay. Fig. 7 summarizes all Zone-1 case results in a bar graph. The relay operates according to the expected times (less than two cycles) for all the cases.

Three cases are chosen for a detailed inspection. They all correspond to a strong power grid and 200 MW WT Type-3. The fault is at 75 % L-I and 50 % L-II, both measured from the relay location in Bus 6.

Case 1, a single-phase-to-ground fault AG at L-I and a phase-to-phase fault AB in L-II occur at the same instant;
Case 2, a single phase-to-ground fault AG at L-I; 0.1 s later, a single phase-to-ground fault CG in L-II; and

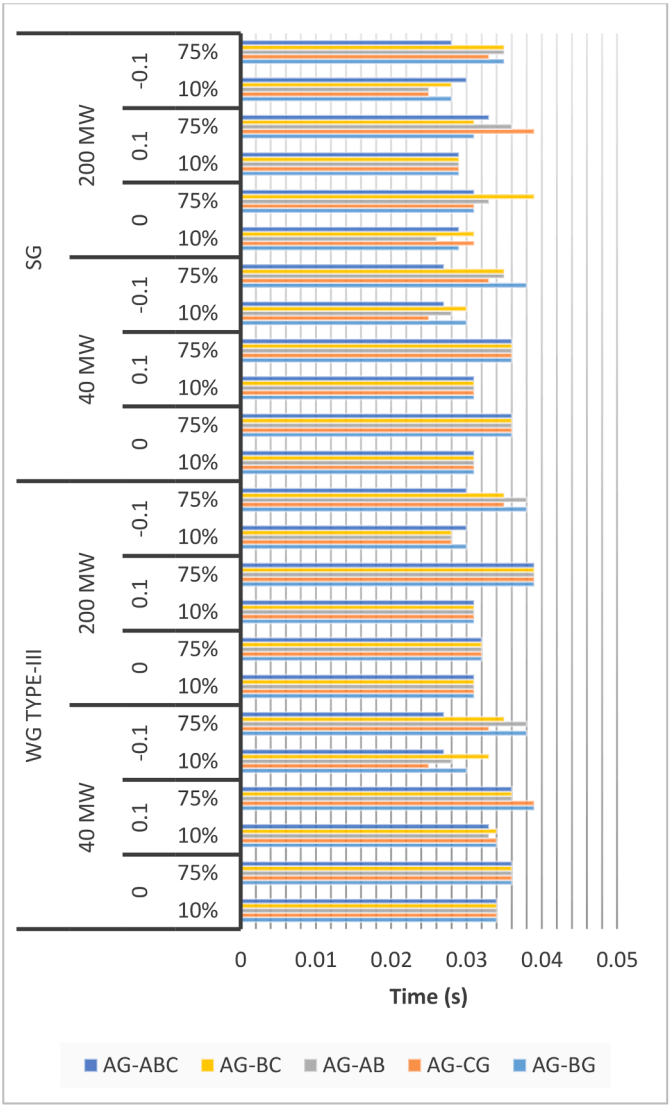

Fig. 7. Study case trip times comparison. (SG synchronous generator vs WG type-III generator).

Case 3, a three-phase fault ABC in L-II; and 0.1 s later, a single-phase-to-ground fault AG in L-I.

4.2. Study case WT `Type III at bus 6

Fig. 8 shows currents detected by the relay, and Fig. 9 shows voltages at bus six. The fault inception times, the circuit breaker (CB_A) opening, and the fault variations are highlighted accordingly. As expected, for cases 1 and 2, during the fault occurrence, a current increase in phase A occurs (Fig. 8(a) and (b)).

For case 3, the ABC fault starts in L-II. The current increase is not as noticeable as in cases 1 and 2. However, in this case, the three-phase fault current increases to the maximum allowed value, and it is limited by the converter. The second fault (AG) occurs at 0.1 s later in L-I. This method allows only the breaker pole of phase A to be opened during a single-phase fault. A memory voltage polarization is used that lasts for five cycles until a fault is completely identified.

The SE in a semi-logarithmic scale is shown in Fig. 10. For case 1 and case 2, the faulty phase SE becomes higher than the SE of the other phases. For case 3, the SE for all phases rises above the threshold when the fault occurs in L-II.

The SE is within the threshold as fast as in cases 1 and 2. However, it operates after 12 ms. The sampling frequency used in this analysis is 500 Hz, and the recursive window contains ten samples. Because the ST is processed recursively, using a window size power of two is unnecessary.

Fig. 11 shows the phase selection depicted by the binary signals. Due to the complexity of the studied fault cases, the phase selector is not as straightforward as expected. However, the indication does not fail and successfully determines the faulty loop in all cases. The same sampling frequency used for the fault detector is also used for the phase selector. Both modules are included in the RTDS as algorithms programmed in C-language.

Case 1, Fig. 11(a) shows that the phase selector detects as first the AG fault. After the corresponding circuit breaker is open, the second fault remains in L-II, and the indicator detects a BG and a BC fault. The fault is AG in L-I and AB in L-II. This is a specific case that validates the proper phase selector operation. For case 2, Fig. 11 (b), the phase selector clearly detects the faulty phase (AG). For case 3, Fig. 11(c), the phase selector detects ABC fault first. This three-phase fault is in the non-protected line L-II. Then, after 0.1 s, an AG fault occurs in the protected line L-I, and the indicator successfully detects the faulty phase. The faulty phase module is realized after three consecutive detections as seen in Fig. 5. Thus, the spikes seen in Fig. 11 are not considered.

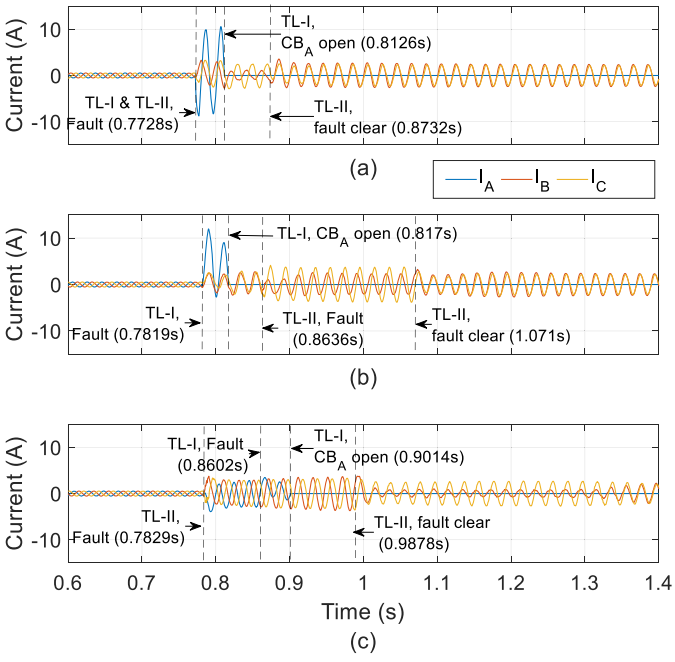

Fig. 8. Study case currents at the relay 6 (a) case 1, (b) case 2, and (c) case 3.

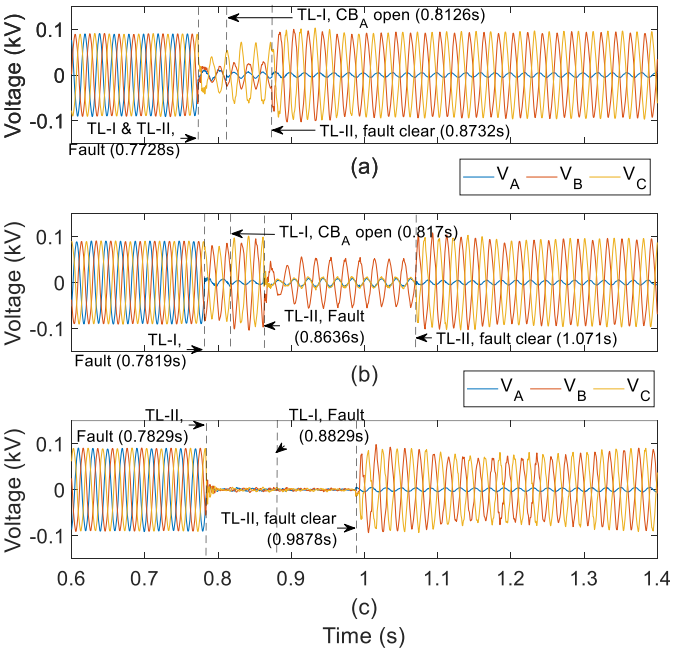

Fig. 9. Study case voltages at bus 6 (a) case 1, (b) case 2, and (c) case 3.

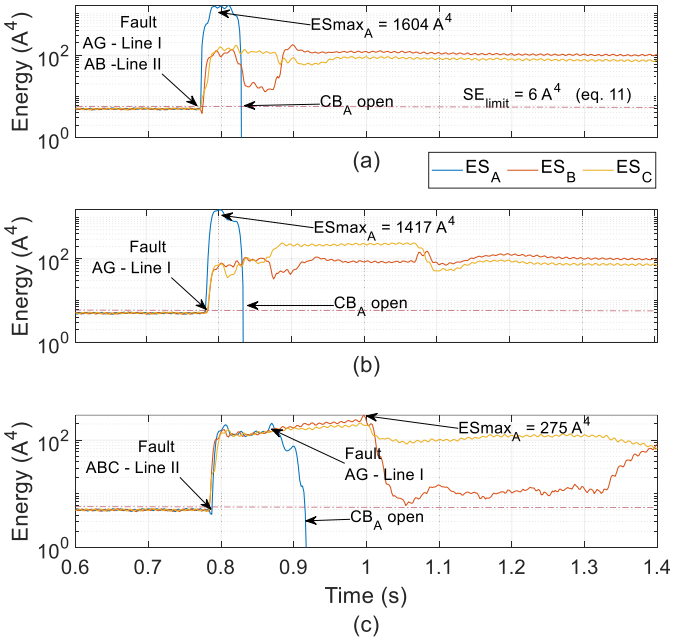

Fig. 10. Study case SE at bus 6 (a) case 1, (b) case 2, and (c) case 3.

The directionality is determined after the phase selection. It comprises three angle comparisons: zero-sequence angle, negative angle, and negative vs. zero angles, as explained in Roberts and Guzman [26]. The fault is in the forward direction when the three angles are lower than the threshold. Otherwise, the fault direction is not determined or reversed. This module is sufficient to determine the fault direction for all 540 cases simulated. Fig. 12 shows the direction angles of the three studied cases.

Therefore, for the three cases, the direction angles named as 3I°, I⁻,

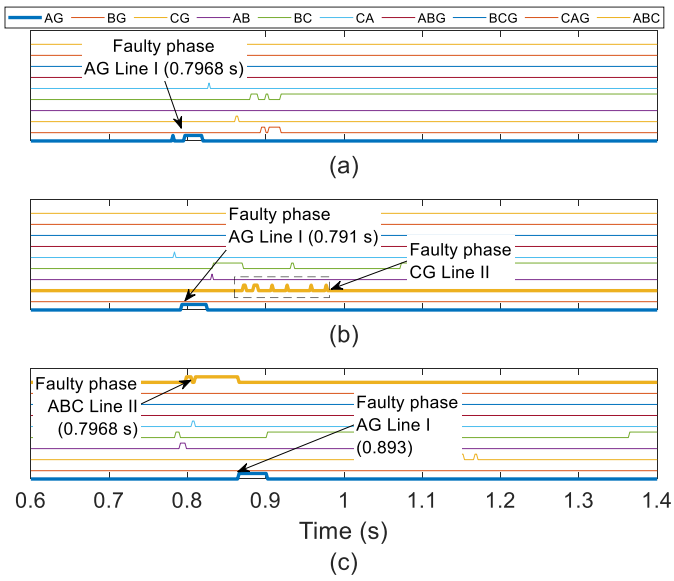

Fig. 11. Study case faulted phase selection relay performance at bus 6 (a) case 1, (b) case 2, and (c) case 3.

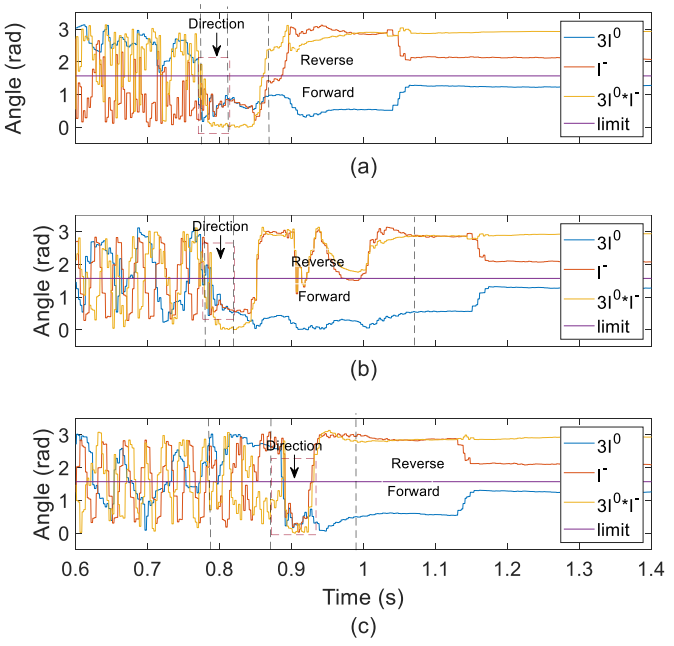

Fig. 12. Study case directional angles for L-I phase A-G loop (a) case 1, (b) case 2, and (c) case 3.

and I°*I⁻ in Fig. 12 are lower than the threshold value, which is equal to π during the fault identification. Thus, the fault is identified as a forward AG fault. For case 3, the first fault is determined as the reverse fault. However, the angles drop when the AG fault is detected along with the faulty phase, indicating a forward fault.

The quadrilateral characteristic is used for single-phase faults, and the impedance trajectory is shown in Fig. 13. For all cases, the black line corresponding to the AG trajectory drops inside Zone-1. Once the fault is fully identified, the trip command is provided, as seen in the flow chart of Fig. 4. Other impedance trajectories, which do not correspond to the fault and are not detected by the phase selector and the directionality module, are also seen in Fig. 12 as informational only.

A good performance is also shown for faults in Zone 2. However, there is some unexpected behavior in the cases when using a strong

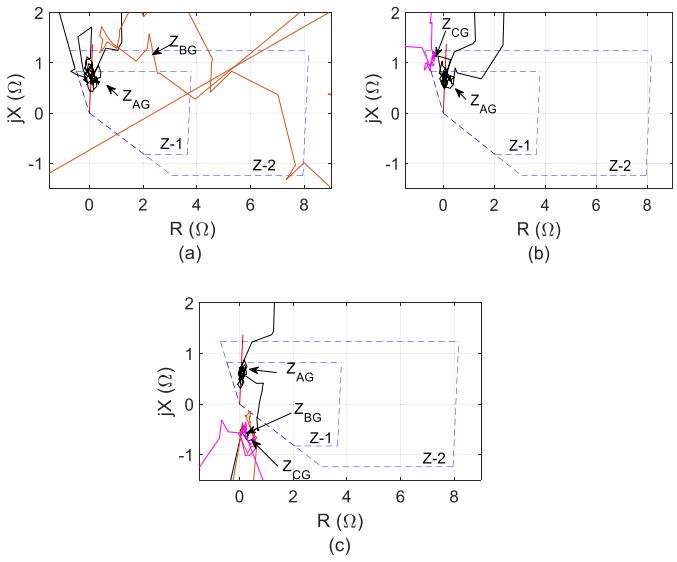

Fig. 13. Study case Impedance trajectory at bus 6 (a) case 1, (b) case 2, and (c) case.

power grid; 200 MW of infeed power and a fault at 90 % of the line. The trip command is activated during these cases as a Zone-1 delayed trip. The pickup, phase selection, and directionality functions show correct performance. However, a few cases during an LL fault in Zone-2 are recorded as relay underreach. In all cases, the fault is identified in less than 40 ms. The exception occurs in cases with a strong power grid, 200 MW infeed power, and a fault at 90 % of the line. In such cases, the impedance computation requires more than 150 ms to enter the quadrilateral characteristic. Three cases are chosen for a detailed inspection. They all correspond to a strong power grid and 200 MW WT Type-3.

4.3. Study case WT `Type IV at bus 6

There is no unique inverted base resource structure, and different topologies behave differently during events. This work also tests the proposed methodology when a WT type-IV or a PVs is connected on bus 6 (see Fig. 6) instead of WT type-III. The IBR uses a full converter based on a pair of three-phase, three-level voltage source converters [29]. The same scenarios used for WT type-III in Section 2.3. In Fig. 14, the trip times are summarised. For all cases, the method achieves correct trip times no greater than 0.035 s at zone-1.

The signals for case 1, when a single-phase-to-ground fault AG at L-I and simultaneously a phase-to-phase fault AB in L-II occurs are presented in Fig. 15(a). It can be seen that the fault detection by the s-transform does not operate even though it is lower in magnitude (as in Fig. 16(a)) than the one provided by WT Type-III (see Fig. 8 (a)). Generally, the faulty phase selection (see Fig. 16(b)) is faster than in the cases where WT type-III is connected. The electronic control used by the WT type-IV is faster than the one used by WT type-III, thus providing signals with less distortion. The fault direction and zone determination for the case are also exposed in Fig. 17. The cases when the fault is at zone 2 are also well determined. The proposed methodology, with its efficient fault detection and clear fault identification, consistently does not operate in identifying the fault when a type-IV is connected.

Fault impedance significantly determines the faulty zone and directionality on the classical distance elements and the proposed one. A detailed study of the method with different impedances is beyond the scope of the paper and will lead to further research.

5. Comparison with real relays

The identical study cases outlined in Section 4.1 are evaluated by

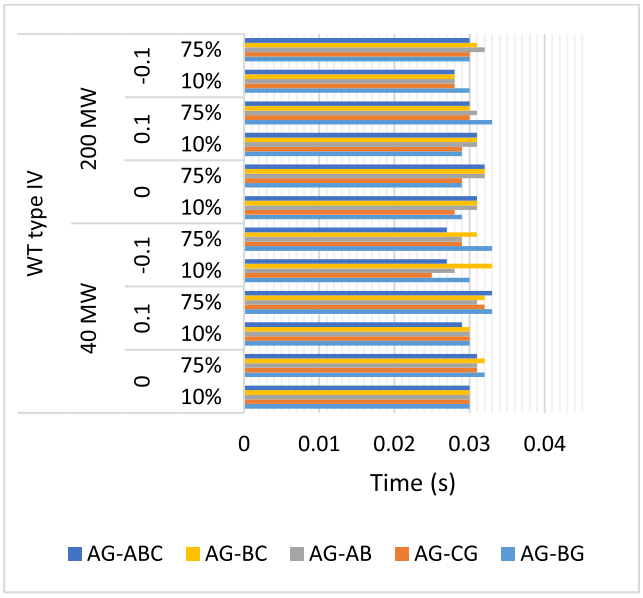

Fig. 14. Trip times summary of all the fault cases with WT type-IV at bus 6 at zone-1.

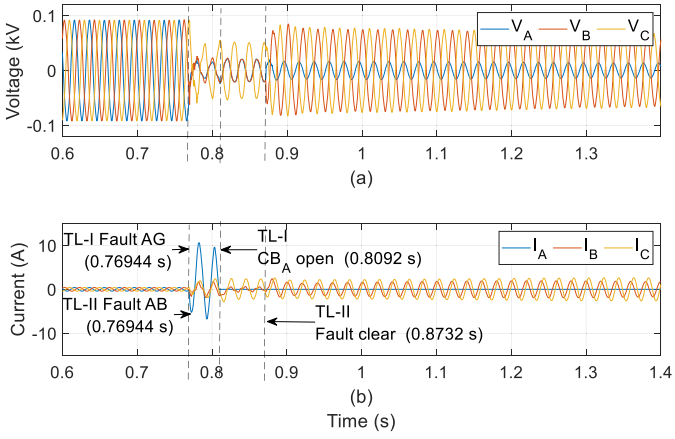

Fig. 15. WT type-IV at bus 6. Case 1 fault AG on line I and AB on line II. (a) voltage in bus 6 and (b) Current in line I.

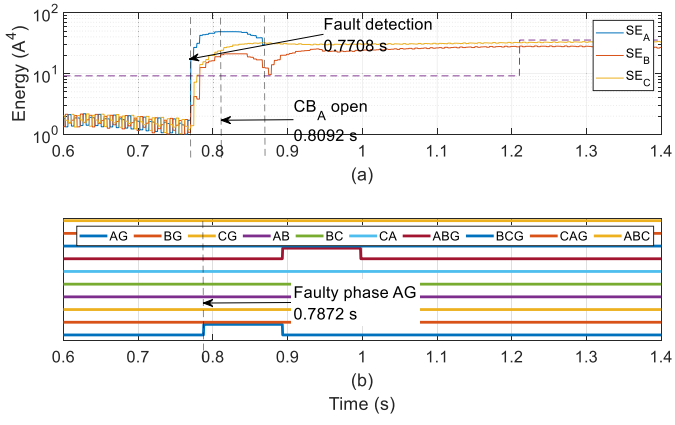

Fig. 16. WT type-IV at bus 6. Case 1 fault AG on line I and AB on line II. (a) fault detection by s energy and (b) faulty phase selection.

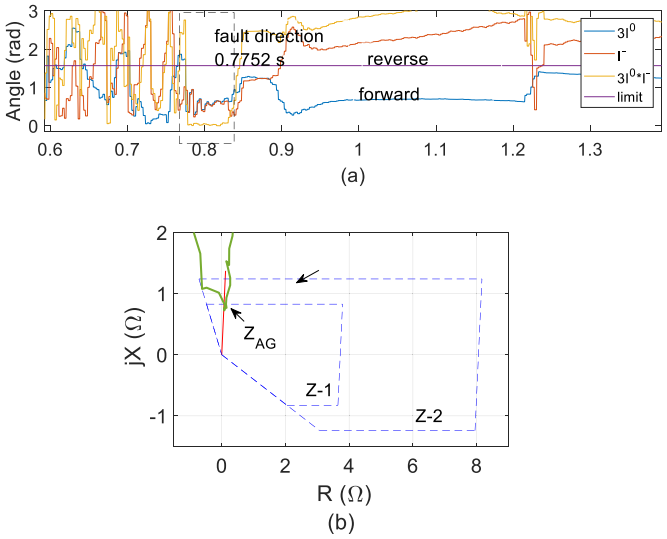

Fig. 17. WT type-IV at bus 6. Case 1 fault AG on line I and AB on line II. (a) fault direction and (b) impedance trajectory.

hardware in the loop test. This evaluation involves using two distinct OMS relays (relay A and relay B) connected in parallel at the same location, as illustrated in Fig. 6, by HiL. The comparison is conducted in terms of the successful execution of tripping commands.

Relays A and B are meticulously calibrated based on the TSO's extensive experience. Given that the study case involves a double circuit line, compensation for a parallel line is applied. Both relays utilize resistance and reactance coupling factors. Relay A's fault detection is done by overcurrent pickup, while the phase selection is achieved through undervoltage detection. Conversely, Relay B's fault detection is executed via a delta algorithm, and phase selection is determined by superimposed values.

The results show that both relays perform correct fault identification and tripping when a synchronous generator is connected at bus 6. However, the scenario changes when the DFIG is on bus 6; in this case, the relays present three scenarios. Case I, relays successfully identify the fault, exempt relay A fault type AG in L-I and ABC in L-II. In this case, the relay fails to determine the single-phase fault, generating a three-phase tripping. In case II, no issues are presented during this scenario, relays are blinded to the fault at the parallel line. For Case III, relays present a low percentage of successful tripping commands, namely no-tripping overreach or delay trips. The performance of the relays versus the proposed methodology can be done by comparing Figs. 18 and 7. In Fig. 18; the y-label axes refer to 1- correct tripping, 2-three phase trip, incorrect phase selection, 3-Overreach, 4- non-tripping. Meanwhile, the proposed methodology presents only correct trips.

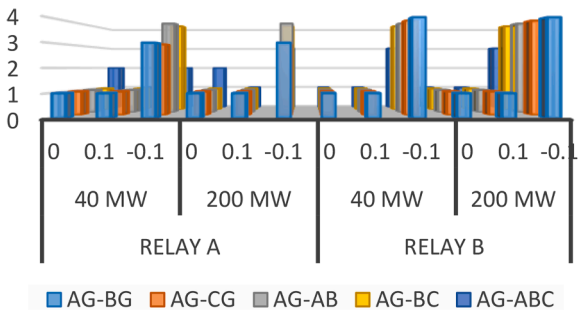

Fig. 18. Real relays performance for WT-Type III, Case I, II, and III.

6. The effect of the grid code; voltage support during and after faults

Dynamic voltage support is mandatory during short-term voltage drops or rises [33]. The relation between the voltage drop/rise and the current support is linear (see Fig. 15(a)).

During voltage drops equal to 50 % of the steady-state value, the IBRs inject at least 1.0 pu reactive current, while during overvoltage, reactive current withdrawal is required. A dead band of 10 % is considered to avoid undesirable control actions. After the voltage level returns to the dead band, the specified IBR characteristic must maintain the voltage support for 500 ms. The transient balancing procedures following the voltage return must be completed after 300 ms. The study cases considered in Section 5, obey this voltage-current support. The current support by the positive and negative currents may arise some issues in traditional fault classification methods which are based on the phase difference between the symmetrical components of the currents or the superimposed values of the phase currents.

In addition, the grid code determines low-voltage ride-through, which is related to the disconnection of the generation plant from the grid, as seen in Fig. 19(a). Only in cases of a fault lasting more than 150 ms and with a nearly zero voltage deep, the IBR should switch to a blocking condition and be disconnected from the system. However, this paper does not consider this specific part of the grid code.

Five additional grid codes used in, Spain, Germany, Denmark, China, and Brazil are used in the same study cases described in Section 4.1 to identify a possible drawback of the proposed method. The dynamic current requirements are shown in Fig. 20.

More than 270 cases per grid code are simulated, and the cases are listed in Section 4.1. Hence a total of 1350 cases are evaluated. Using the proposed technique, all faults are identified. The proposed technique determines the start of the fault by comparing the s-energy against self-determined limits (See Section 3.1); all faults are detected in less than 15 ms. For phase selection using the s-energy method as an identifier as explained in Section 3.2. The proposed fault detection and phase selection are immune to grid code requirements.

Current transformers (CT) and voltage transformers (VT) are modelled as ideal transformers, and their performance is not investigated. The CTs ratio is 200A/5 A, and the VTs are 440 kV/100 V. These ratios are for the physical relays and for the proposed method.

7. Comparison with other fault identification methods

The proposed method is meticulously compared with six recently proposed approaches, including compensation with symmetrical components [11], maximal overlap discrete wavelet transform [9], fast discreet orthonormal Transform plus pattern recognition [17], discrete Fourier transform and transient monitor index [19], variational mode decomposition and convolutional neural network [21], and a

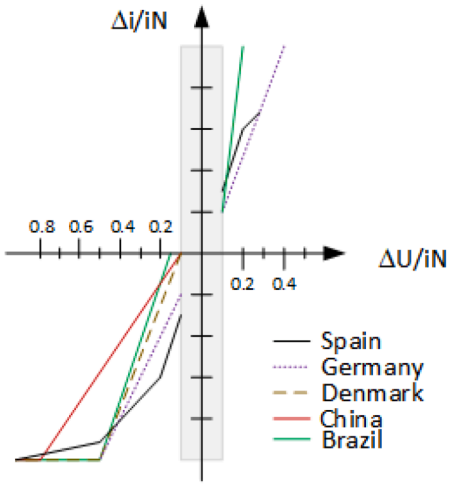

Fig. 20. Dynamic current requirements for different countries.

combination of voltage and current symmetrical components [22]. These methods have been used for cross-country faults, faults at lines near IBRs, lines near power flow controllers, or a combination of two of them.

Table 2 summarizes the comparative results considering different essential features. The table reveals the high accuracy of the proposed method and its superiority in terms of the sampling frequency used. In terms of fault, classification and immunity to different factors are competitive; it also shows that compared to others, the method has covered the faults near WT type-III, WT type-IV, and solar farms, demonstrating its potential for real-world applications.

8. Conclusions

A new method for fault detection and faulty phase selection has been presented. The techniques developed based on the Recursive Discrete Stockwell Transform (RDST) help to decrease the computational burden and speed up the execution time by reducing the total number of operations, especially after the first iteration. The main reason for using the Stockwell Energy (SE) as a fault detector is its high sensitivity to distortion produced during faults. This feature is quite advantageous, especially for faults near inverter-based Resources (IBR), which limit the fault current magnitude. Another advantage of using the RDST is the flexibility to use any number of samples per window without a meaningful impact on the overall speed. The number of samples does not need to be with a power of two sizes.

The proposed faulty phase selector module takes advantage of the RDST to enable the identification of the faulty phase; its most significant advantage is ground fault detection. The zero-sequence commonly

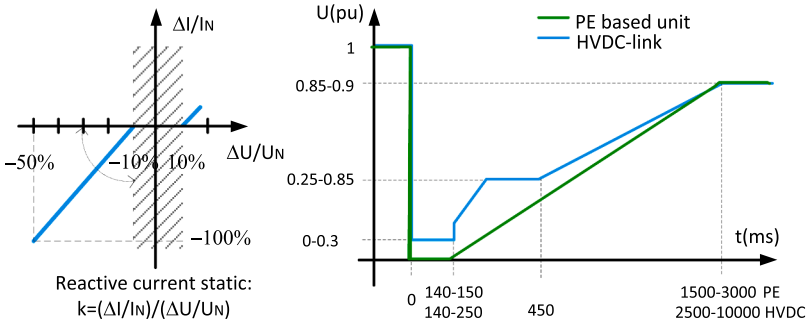

Fig. 19. Grid code a) Dynamic current requirements and b) Low voltage ride through.

Table 2
Proposed method comparison whit other approaches.

Method	System and sampling frequency	Data use	IBR in the system or Power flow controller (PFC)		Cross country test	Detection accuracy	Classification accuracy		Identification time
			IBR type	PFC type			First zone	Second Zone.	
[11]	50 Hz / 60 Hz Any res	Voltage and current	No	No	Yes	100 %	100 %	100 %	ND
[9]	50 Hz 1 kHz, 1.2 kHz, 10 Kz, 20 kHz	Voltage and current	No	No	Yes	100 %	100%	100 %	~12.5
[17]	60 Hz 3 kHz	Voltage and current	No	UPFC	No	98.88 %	100 %	NT	~ND
[19]	50 Hz 1 kHz	Current	WT Type III	UPFC	No	100 %	99.24 %	NT	~ 20 ms
[21]	50 Hz, 4 kHz	Current	WT 'Type III	UPFC	No	100 %	99.78 %	99.78	~15 ms
[22]	60 Hz 2 kHz	Voltage and current	WT type IV Solar farm	No	No	100 %	100%	NT	~40 ms
Proposed	50 Hz, 0.5 kHz	Current	WT Type III WT. Type IV Solar farm	No	Yes	100 %	100 %	98.5 %	~17 ms

Method	Real time tested	Inaccuracies due to:				
		Load, Cap-Switch.	Noice	CT Sat-	Grid code	v/i inversion
[11]	No	No	NT	NT	NT	NT
[9]	Yes	No	No	No	NT	No
[17]	No	NT	NT	NT	NT	NT
[19]	Yes	No	No	NT	NT	No
[21]	Yes	No	No	No	NT	No
[22]	No	No	No	No	No	NT
Proposed	Yes	No	No	NT	No	No

ND, No data; NT, No tested.

performs ground detection outside the faulty phase detector module. The proposed method can detect ground faults during cross-country faults (CCF) within a half cycle following the fault onset. These cases are traditionally quite challenging, especially for the phase selection and directionality modules. However, the phase selector based on the SE and the directionality based on classical sequence angles perform correctly for all simulated cases. The proposed method has been implemented in real-time, corroborating the feasibility of implementing it on real devices.

CRediT authorship contribution statement

Jose de Jesus Chavez: Writing – review & editing, Writing – original draft, Visualization, Validation, Supervision, Software, Resources, Project administration, Methodology, Investigation, Formal analysis, Data curation, Conceptualization. **Marjan Popov:** Writing – review & editing, Supervision, Project administration, Formal analysis, Conceptualization. **David López:** Writing – review & editing, Resources, Investigation, Formal analysis, Data curation. **Vladimir Terzija:** Writing – review & editing, Validation, Supervision, Formal analysis, Conceptualization. **Sadegh Azizi:** Writing – review & editing, Validation, Formal analysis, Data curation, Conceptualization.

Declaration of competing interest

The authors declare that they have no known competing financial interests or personal relationships that could have appeared to influence the work reported in this paper.

Data availability

Data will be made available on request.

Appendix A

The inverted base resources used in this paper correspond to Wind turbine type-3, type-4, and solar photovoltaic. The full-converted (FC) model is used for wind turbine type-4 and solar photovoltaic IBRs. The IBR models are explained in detail in the Horizon 2020 MIGRATE project [28].

WT type-3 comprises an induction generator, crowbar, chopper, grid voltage source converter (VSC), and rotor VSC. The VSC contains four inner controllers. Two regulate the positive sequence of the current components, while the others control the negative sequence [30]. The positive sequence outer controllers in grid VSC maintain a constant DC-link voltage and provide the required reactive power (as a STATCOM) at the DFIG point of common coupling (PCC) as specified in the TenneT grid code. Simultaneously, the rotor VSC positive sequence outer controllers regulate the active and reactive power based on the optimal wind turbine power extraction and the applied grid code. Likewise, in the positive sequence controllers, four regulators are considered to control the negative sequence current component. Different control strategies, each with its own unique, can be applied to provide reference control signals for the negative sequence regulators. The chosen control strategy is double-frequency minimization [31]. VSC's positive and negative sequence controls are implemented in the inner loop, as shown in the following schematic figures. The use of elaborate control

produces a natural delay once Real-Time simulation is used. Thus, there is no need to include delays in the control models [32]. This is not the case for mechanical elements; in this sense, the circuit breaker model has 50ms to reproduce the mechanical behavior (Fig. 21).

WT type-4 and PV are connected to the system by a full converter; WT type-4 is composed of a permanent magnet synchronous generator, and the control used focuses on the double-frequency minimization and negative sequence. During the normal state of the system, without an event, the output current is controlled only by a positive sequence component [29]. However, when an event is in the system, the negative sequence is provided proportionally to the positive sequence, considering the allowed fault current limits. The other control loop for the full converter is shown in Fig. 22 [4]. It can be seen the positive and negative control modules.

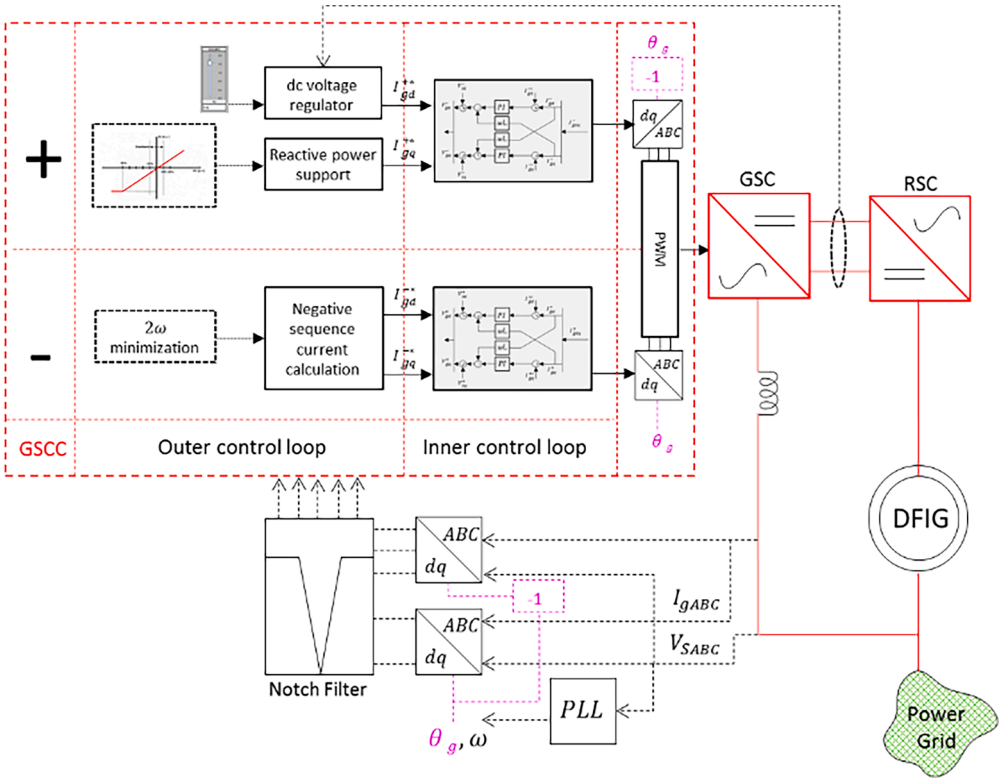

Fig. 21. Outer control loops, inner control loops, and the required measurements for the wind turbine type-3 GSC.

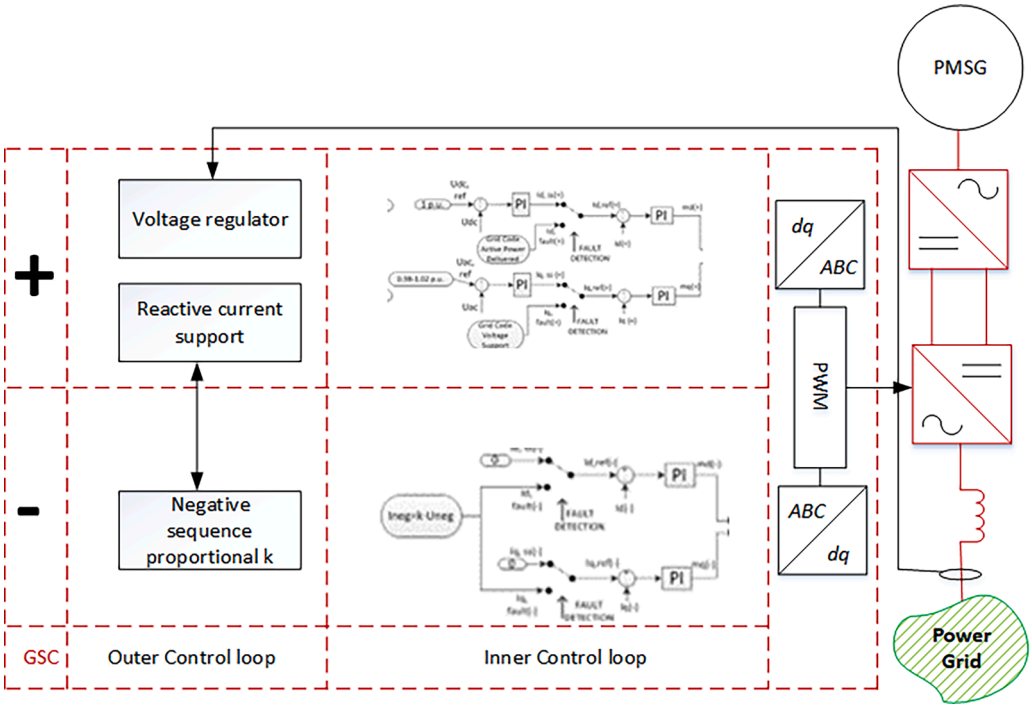

Fig. 22. Outer control loops, inner control loops, and the required measurements for the full converter GSC.

Appendix B

The transmission line characteristic is as follows (Table 3).

Table 3
Transmission line model.

Parameter	Quantity
Model	Bergeron
Line length	30 km
Frequency	50 Hz
Positive sequence series resistance	0.0293 Ω/km
Positive sequence series induction reactance	0.3087 Ω/km
Positive sequence shunt capacitance reactance	0.2664 MΩ/km
Zero sequence series resistance	0.300 Ω/km
Zero sequence series induction reactance	0.988 Ω/km
Zero sequence shunt capacitance reactance	0.4369 MΩ/km
Transposition	Zero sequence coupling
Mutual resistance	0.162 Ω/km
Mutual reactance	0.781 Ω/km

References

[1] J. Andruszkiewicz, J. Lorenc, B. Staszak, A. Weychan, B. Zięba, Overcurrent protection against multi-phase faults in MV networks based on negative and zero sequence criteria, Int. J. Electr. Power Energy Syst. 134 (2022) 1–11.

[2] P. Chang, G. Song, J. Hou, R. Xu, A novel voltage phase selector for inverter-interfaced system based on two-stage control strategy, Int. J. Electr. Power Energy Syst. 133 (2021) 1–12.

[3] P. Horton, S. Swain, Using superimposed principles (delta) in protection techniques in an increasingly challenging power network, in: *70th Annual Conference for Protective Relay Engineers* (CPRE), 2017.

[4] E. Martínez Carrasco, M.P. Comech Moreno, M.T. Villén Martínez, S. Borroy Vicente, Improved faulted phase selection algorithm for distance protection under high penetration of renewable energies, Energies 13 (3) (2020) 55.

[5] K. Solak, W. Rebizant, Analysis of differential protection response for cross-country faults in transmission lines, in: Proc. Modern Electric Power Systems (MEPS), 2010, pp. 1–4.

[6] A. Zin, N.A. Omar, A.M. Yusof, S. Karim, Effect of 132 kV cross-country fault on distance protection system, in: Proc. Asia Modelling Symposium (AMS), 2012, pp. 167–172.

[7] Z.Y. Xu, W. Li, T.S. Bi, G. Xu, Q.X. Yang, First-zone distance relaying algorithm of parallel transmission lines for cross-country nonearthed faults, IEEE Trans. Power Deliv. 26 (Oct. 2011) 2486–2494.

[8] T. Bi, W. Li, Z. Xu, Q. Yang, First-zone distance relaying algorithm of parallel transmission lines for cross-country grounded faults, IEEE Trans. Power Deliv. 27 (2012) 2185–2192.

[9] V. Ashoka, A. Yadava, A.Y. Abdelaziz, MODWT-based fault detection and classification scheme for cross-country and evolving faults, Electr. Power Syst. Res. 175 (2019) 105897.

[10] A. Borgnino, M. Castillo, Comparison of the performance of different directional polarizing methods in cross country fault protection of an MV loop, in: Proc. 2018 Power Systems Computation Conference (PSCC), 2018, pp. 1–7.

[11] C. Venkatesh, I. Voloh, Cross country faults - protection challenges and improvements, in: Proc. Protective Relay Engineers (CPRE) Conf, 2021, pp. 1–15.

[12] G.M.G. Guerreiro, Z. Gajić, S. Zubić, N. Taylor, Md Z. Habib, Cross-Country faults in resonant-grounded networks: Mathematical modelling, simulations and field recordings, Electr. Power Syst. Res. 196 (2021) 107240.

[13] S. Biswas, P.K. Nayak, State-of-the-art on the protection of FACTS compensated high-voltage transmission lines: a review, IET High Volt. 3 (1) (2018) 21–30.

[14] A. Haddadi, E. Farantatos, I. Kocar, U. Karaagac, Impact of inverter based resources on system protection, Energies 14 (4) (2021) 1050.

[15] L. He, C.C. Liu, A. Pitto, D. Cirio, Distance protection of AC grid with HVDC-connected offshore wind generators, IEEE Trans. Power Deliv. 29 (2) (2014) 493–501.

[16] A. Hooshyar, E.F. El-Saadany, M. Sanaye-Pasand, Fault type classification in microgrids including photovoltaic DGs, IEEE Trans. Smart Grid 7 (5) (2015) 2218–2229.

[17] Z. Moravej, M. Pazoki, M. Khederzadeh, New pattern-recognition method for fault analysis in transmission line with UPFC, IEEE Trans. Power Deliv. 30 (3) (2015) 1231–1242.

[18] M.A. Azzouz, A. Hooshyar, E.F. El-Saadany, Resilience enhancement of microgrids with inverter-interfaced DGs by enabling faulty phase selection, IEEE Trans. Smart Grid 9 (6) (2017) 6578–6589.

[19] S. Biswas, P.K. Nayak, A fault detection and classification scheme for unified power flow controller compensated transmission lines connecting wind farms, IEEE Syst. J. 15 (2021) 297–306.

[20] S. Biswas, P.K. Nayak, G. Pradhan, A dual-time transform assisted intelligent relaying scheme for the STATCOM-compensated transmission line connecting wind farm, IEEE Syst. J. 16 (2) (2022) 2160–2171.

[21] S. Biswas, P.K. Nayak, B.K. Panigrahi, G. Pradhan, An intelligent fault detection and classification technique based on variational mode decomposition-CNN for transmission lines installed with UPFC and wind farm, Electr. Power Syst. Res. 223 (2023) 1–15.

[22] M.M. Mobashsher, A.A. Abdoos, S.M. Hosseini, S.M. Hashemi, M. Sanaye-Pasand, A new fault type classification method in the presence of inverter-based resources, Int. J. Electr. Power Energy Syst. 147 (2023) 108793.

[23] J.J. Chavez, M. Popov, D. López, S. Azizi, V. Terzija, S-transform based fault detection algorithm for enhancing distance protection performance, Int. J. Electr. Power Energy Syst. 130 (2021) 106966.

[24] K.R. Krishnanad, P.K. Dash, A new real-time discrete S-transform for cross-differential protection of shunt-compensated power systems, IEEE Trans. Power Syst. 28 (2013) 402–410.

[25] T. Nguyen, Y. Liao, Power quality disturbance classification utilizing S-transform and binary feature matrix method, Electr. Power Syst. Res. 79 (2009) 569–575.

[26] J. Roberts, A. Guzman, Directional element design and evaluation, in: Proc. 21st Annual Western Protective Relay Conference, 1994, pp. 1–28.

[27] E.O. Schweitzer, J. Roberts, Distance relay element design, SEL J. Reliab. Power 1 (2010) 1–18.

[28] M. Popov, J. Chavez, et al., Enhancing distance protection performance in transmission systems with renewable energy utilization, in: *Proc. IEEE PES Innovative Smart Grid Technologies Europe* (ISGT-Europe), 2020, pp. 181–185.

[29] W.-S. Oh, S.-K. Han, S.-W. Choi, G.-W. Moon, Three phase three-level PWM switched voltage source inverter with zero neutral point potential, IEEE Trans. Power Electron. 21 (5) (2006) 1320–1327.

[30] R. Chowdhury, N. Fischer, Transmission line protection for systems with inverter-based resources—Part I: problems, IEEE Trans. Power Deliv. 36 (4) (2021) 2416–2425.

[31] L. Xu, Coordinated control of DFIG's rotor and grid side converters during network unbalanced, IEEE Trans. Power Electron. 23 (2008) 1041–1049.

[32] NERC, Reliability Guideline BPS-Connected Inverter-Based Resource Performance 2018.

[33] EC–European Commission, Establishing a Network Code on Requirements for Grid Connection of Generators, European Commission, Brussels, Belgium, 2016.

Jose de Jesus Chavez received the M.Sc. and Ph.D. degrees from the Center for Research and Advanced Studies, National Polytechnic Institute, Mexico City, in 2006 and 2009, respectively. In 2009, he joined the RTX-LAB, University of Alberta, as a Visiting Ph.D. Student. He joined the Technological Institute of Morelia, Mexico, as an Assistant Professor in 2010, where he was a Full Professor in 2012 and the Chair of the Graduate and Research Program in electrical engineering from 2014 to 2016. He was a Post-Doctoral Member with TU Delft, the Netherlands, from 2016 to 2020 and a guest researcher since 2021. He joined the National Technological Institute of Mexico (TecNM) from 2020 to 2022. Since 2023, he is with the Tecnologico de Monterrey, School of Engineering and Sciences campus Guadalajara as a research-proffessor. He is an Associate Editor for Elsevier's e-Prime - Advances in Electrical Engineering, Electronics and Energy. His research interests include power systems primary protection, wide area protection, digital protective relays, and real-time simulation.

Marjan Popov obtained his Ph.D. in electrical power engineering from the Delft University of Technology, Delft in 2002 where he is a professor in power system protection. He is also a Chevening Alumnus and, in 1997, he was an Academic Visitor with the University of Liverpool, Liverpool, U.K., working in the Arc Research Group on modeling SF6 circuit breakers. His major fields of interest are future power systems, large-scale power system transients, intelligent protection for future power systems, and wide-area monitoring and protection. He is a member of Cigre and actively participated in WG C4.502 and WG A2/C4.39. In 2010, he received the prestigious Dutch Hidde Nijland Prize for extraordinary research achievements. He was the recipient of the IEEE PES Prize Paper Award and IEEE Switchgear Committee Award in 2011. He is a Co-Editor-in-Chief for Elsevier's e-Prime - Advances in Electrical Engineering, Electronics and Energy and an Associate Editor for Elsevier's International Journal of Electrical Power and Energy Systems. In 2017, together with the Dutch utilities TenneT, Alliander, and Stedin, he founded the Dutch Power System Protection Centre to promote research and education in power system protection.

David López Cortón received his Master's Degree in Industrial Engineering, specialty Electrical Engineering, by the Polytechnique University of Madrid (UPM), Spain. In 2009, he joined Red Eléctrica (A Redeia Group Company), the Spanish TSO, as dispatcher of the national control room. In 2013, he moved to the System Security Department of Red Eléctrica, where he held different responsibilities including the Technical Direction of the Testing and Calibration Laboratory, being responsible for protection testing, qualification of new protection equipment, validation of protection and automation schemes, disturbance root cause analysis, and metrology. In 2022, he moved to Redinter Chile (A Redeia Group Company) as Manager of Strategy and Planning for Redinter and TEN.

Vladimir Terzija was born in Donji Baraci (former Yugoslavia). He received the Dipl-Ing., M.Sc., and Ph.D. degrees in electrical engineering from the University of Belgrade, Belgrade, Serbia, in 1988, 1993, and 1997, respectively. He is a Professor of Energy Systems & Networks at the Newcastle University, UK. He is also a Distinguished Visiting Professor at Shandong University, China, as well as a Guest Professor at the Technical University of Munich, Germany. In the period 2021–2023 he was a Full Professor at Skoltech, Russian Federation. In the period 2006–2020 he was the EPSRC Chair Professor at The University of Manchester, UK. From 2000 to 2006, he was a Senior Specialist for switchgear and distribution automation with ABB, Ratingen, Germany. From 1997 to 1999, he was an Associate Professor with the University of Belgrade, Belgrade, Serbia. His current research interests include smart grid applications, wide-area monitoring, protection and control, multi-energy systems, transient processes, ICT, data analytics, and complex science applications in power systems. He is the Editor-in-Chief of the *International Journal of Electrical Power and Energy Systems*, Humboldt Fellow and the recipient of the National Friendship Award, China.

Sadegh Azizi received the B.Sc. degree from K. N. Toosi University of Technology, Tehran, Iran, in 2007, the M.Sc. degree from Sharif University of Technology, Tehran, Iran, in 2010, and the Ph.D. degree from University of Tehran, Tehran, Iran, in 2016, all in electrical power engineering. He is currently a Lecturer in Smart Energy Systems with the School of Electronic and Electrical Engineering, University of Leeds, Leeds, U.K. From June 2016 to January 2019, he was with The University of Manchester as a Postdoctoral Researcher leading their work on the protection Work Package of the EU H2020 MIGRATE project, in collaboration with more than 20 European Transmission System Operators and research institutes. He was with the Energy and System Study Center, Monenco Iran Consulting Engineers Co., from 2009 to 2011, and the Iran Grid Management Co., Tehran, Iran, from 2013 to 2016. He is an Associate Editor for the *International Journal of Electrical Power and Energy Systems*. He is also a Task Leader of Cigré WG B5.57, which is investigating new challenges of frequency protection in modern power systems. His research interests include wide-area monitoring, protection and control systems, digital protective relays, and applications of power electronics in power systems.